# A mitochondrial ADXR–ADX–P450 electron transport chain is essential for maternal gametophytic control of embryogenesis in *Arabidopsis*

Andrés Martin Bellido[a,1], Ayelén Mariana Distéfano[a,1], Nicolás Setzes[a,1], María Milagros Cascallares[a], Jana Oklestkova[b], Ondrej Novak[b], Javier Alberto Ramirez[c,d], Eduardo J. Zabaleta[a], Diego F. Fiol[a], and Gabriela C. Pagnussat[a,2]

[a]Instituto de Investigaciones Biológicas, Universidad Nacional de Mar del Plata, Consejo Nacional de Investigaciones Científicas y Técnicas (CONICET), 7600 Mar del Plata, Argentina; [b]Laboratory of Growth Regulators, Faculty of Science, Institute of Experimental Botany and Palacký University, The Czech Academy of Sciences, 78371 Olomouc, Czech Republic; [c]Departamento de Química Orgánica, Facultad de Ciencias Exactas y Naturales, Universidad de Buenos Aires, C1428EGA Ciudad Autónoma de Buenos Aires, Argentina; and [d]Unidad de Microanálisis y Métodos Físicos Aplicados a Química Orgánica (UMYMFOR), Universidad de Buenos Aires, CONICET, C1428EGA Ciudad Autónoma de Buenos Aires, Argentina

Edited by Ravishankar Palanivelu, The University of Arizona, Tucson, AZ; received January 9, 2020; accepted December 11, 2021 by Editorial Board Member Krishna K. Niyogi

**Mitochondrial adrenodoxins (ADXs) are small iron–sulfur proteins with electron transfer properties. In animals, ADXs transfer electrons between an adrenodoxin reductase (ADXR) and mitochondrial P450s, which is crucial for steroidogenesis. Here we show that a plant mitochondrial steroidogenic pathway, dependent on an ADXR–ADX–P450 shuttle, is essential for female gametogenesis and early embryogenesis through a maternal effect. The steroid profile of maternal and gametophytic tissues of wild-type (WT) and *adxr* ovules revealed that homocastasterone is the main steroid present in WT gametophytes and that its levels are reduced in the mutant ovules. The application of exogenous homocastasterone partially rescued *adxr* and P450 mutant phenotypes, indicating that gametophytic homocastasterone biosynthesis is affected in the mutants and that a deficiency of this hormone causes the phenotypic alterations observed. These findings also suggest not only a remarkable similarity between steroid biosynthetic pathways in plants and animals but also a common function during sexual reproduction.**

plant reproduction | gametophyte | homocastasterone | embryogenesis | P450

Mitochondrial ferredoxins, also known as adrenodoxins (ADXs), are small iron–sulfur proteins encoded by nuclear genes that are ubiquitously found in plants, animals, and bacteria. They belong to the large family of [2Fe-2S]–type ferredoxins and have electron transfer properties. In animals, ADXs function as mobile shuttles that transfer electrons between an adrenodoxin reductase (ADXR) and mitochondrial P450s (1–4). The reduction of the mitochondrial cytochrome P450 catalyzed by ADXR is a crucial step that leads to steroidogenesis (3). The name "adrenodoxin" is in fact related to the tissue from which ADX was first isolated: the adrenal glands. In adrenal mitochondria, ADX transfers electrons from the NADPH-dependent ferredoxin reductase ADXR to the P450 CYP11A1 and the enzymes of the CYP11B family. CYP11A1, also known as P450scc, catalyzes three consecutive hydroxylation steps that result in cholesterol side-chain cleavage producing pregnenolone, which is the precursor of all mammalian steroid hormones, including glucocorticoids, mineralocorticoids, and sex steroids (3). The system is also functional in invertebrates. In *Drosophila melanogaster*, ADXR is encoded by the nuclear gene *dare*, and it also plays an essential role in ecdysteroid biosynthesis. Ecdysteroids are steroid hormones that function both in male and female arthropods that are stored in oocytes for use during embryogenesis (4). Null mutants of *dare* undergo developmental arrest that is rescued by feeding mutant larvae with the insect steroid hormone 20-hydroxyecdysone (4). In addition, reduction of *dare* expression affects olfactory-driven behavior, and causes degeneration of adult neurons.

Although two genes encoding for ADX (*ADX1* and *ADX2*) and one gene encoding for an ADXR (*ADXR*) are present in the *Arabidopsis thaliana* genome (5), very little is known about the potential roles for these proteins in plants. Recombinant ADX1 and ADXR proteins are sufficient to transfer electrons from NADPH to cytochrome *c* in vitro (5) and ADXR exhibits kinetics properties and electron source preferences that are similar to those reported for mammalian proteins (6). The only role attributed to the plant ADX–ADXR system so far is the synthesis of biotin. In association with BIO2, an iron–sulfur (Fe-S) cluster enzyme, ADXR and ADX1 form an efficient plant biotin synthase complex in vitro (6). However, no functional/physiological studies have been performed for these proteins in planta and there are no in vivo data about possible reduction partners. One possibility is that the ADX–ADXR system reduces a cytochrome P450 in plant mitochondria, as reported in animal systems. However, even when *A. thaliana* cytochrome P450 proteins are encoded by a divergent superfamily of genes that includes 244 genes and 28 pseudogenes, no mitochondrial P450s were found or at least reported so far.

## Significance

**Mitochondrial adrenodoxins (ADXs) are small iron–sulfur proteins that function as mobile shuttles transferring electrons. Their function has been largely known in animals, as they transfer electrons between an adrenodoxin reductase (ADXR) and mitochondrial P450s, which is a crucial step that leads to steroidogenesis. Here we show that a functional mitochondrial ADX–ADXR–P450 pathway is essential for steroid biosynthesis and that its function is required for plant sexual reproduction.**

Author contributions: J.O., O.N., E.J.Z., D.F.F., and G.C.P. designed research; A.M.B., A.M.D., N.S., M.M.C., J.O., and O.N. performed research; N.S. and J.A.R. contributed new reagents/analytic tools; A.M.B., A.M.D., N.S., J.O., O.N., D.F.F., and G.C.P. analyzed data; and A.M.B., A.M.D., E.J.Z., D.F.F., and G.C.P. wrote the paper.

The authors declare no competing interest.

This article is a PNAS Direct Submission. R.P. is a guest editor invited by the Editorial Board.



[1]A.M.B., A.M.D., and N.S. contributed equally to this work.

[2]To whom correspondence may be addressed. Email: gpagnussat@mdp.edu.ar.

This article contains supporting information online at http://www.pnas.org/lookup/suppl/doi:10.1073/pnas.2000482119/-/DCSupplemental.

Published January 19, 2022.

Here we show that a functional mitochondrial ADX–ADXR–P450 pathway is essential for homocastasterone biosynthesis and that its function is required for plant sexual reproduction. The study of *adxr* mutants and double mutants for *ADX1* and *ADX2* revealed that this electron shuttle is critical for female gametophyte development and for early embryogenesis through a maternal effect. Three mitochondrial cytochrome P450 proteins were identified as ADX1 interactors and triple-mutant plants mimic *adx* and *adxr* mutant phenotypes, suggesting overlapping physiological roles. The study of the steroid profile of maternal and gametophytic tissues of wild-type (WT) and *adxr* ovules revealed that homocastasterone is mostly found in gametophytes and that its levels are reduced in mutant ovules. Moreover, application of exogenous homocastasterone partially rescued the phenotypes of ADXR and cytochrome P450 mutants. Altogether, our results indicate that the mitochondrial shuttle ADX–ADXR–P450 is essential for *Arabidopsis* reproduction and required for homocastasterone biosynthesis in the female gametophyte.

## Results

**ADXs and ADXR Are Essential for Normal Female Gametophyte Development and Early Embryogenesis in *A. thaliana*.** To analyze possible roles for the ADX–ADXR shuttle in *A. thaliana*, two independent insertional lines (Columbia [Col-0] ecotype) with T-DNA insertions located at exon 4 (*adxr-1*) and intron 4 (*adxr-2*) were characterized (*SI Appendix*, Fig. S1). After backcrossing these lines to the Col-0 ecotype, the progeny from self-crossed plants was examined by PCR-based genotyping. No homozygous mutant plants were recovered in the offspring from either *adxr-1*/*ADXR* or *adxr-2*/*ADXR* self-pollinated plants. The ratio of hemizygous to WT plants was 1.05 for *adxr-1*/*ADXR* ($n$ = 449) and 1.23 for *adxr-2*/*ADXR* plants ($n$ = 247). Such ratios, as previously reported, suggest failure to transmit the mutation to the next generation through either the male or female gametophyte (7). As no homozygous *adxr* plants were recovered, only hemizygous mutant plants were analyzed. No obvious sporophytic defects were observed in the hemizygous plants (*SI Appendix*, Fig. S1). However, siliques of *adxr*/*ADXR* plants showed a reduction in seed set of about 35% (Fig. 1 *A* and *B*), suggesting that the gene is essential for gametogenesis and/or seed development. To study the genetic basis of the defect in the seed set observed, we crossed hemizygous plants as either pollen or pistil donors to WT plants from the Columbia accession, and the transmission efficiency (TE; no. of progeny with T-DNA insertion/WT offspring × 100) of *adxr* was calculated (*SI Appendix*, Table S1). Only ∼19% of megagametophytes carrying *adxr-1* and around 30% of megagametophytes carrying *adxr-2* successfully transmitted the insertion to the next generation, showing that the mutation affects female gametophyte development or function. TE through the pollen was ∼88.% for *adxr-1* and 83% for *adxr-2*, suggesting that male gametophytes are not severely affected by the mutation (*SI Appendix*, Table S1).

To analyze how this mutation alters female gametophytes, the terminal phenotype of female gametophytes from emasculated *adxr*/*ADXR* flowers was studied (Fig. 1 *C–F* and *SI Appendix*, Fig. S2 and Table S2). In WT *Arabidopsis*, the female gametophyte is a seven-cell structure that includes two gametic cells (the egg cell and the central cell) and five accessory cells: three antipodal cells of unknown function at the chalazal end of the female gametophyte and two synergid cells that flank the egg cell at the micropylar end. Together, the egg cell and the two synergid cells (responsible for pollen tube attraction) form the egg apparatus (7). While WT pistils only showed 2% of abnormal female gametophytes, *adxr*/*ADXR* pistils showed that around 13% of the ovules were carrying anomalous gametophytes ($n$ = 720 for *adxr-1*/*ADXR* and $n$ = 801 for *adxr-2*/*ADXR*; *SI Appendix*, Table S2). Mutant *adxr-1* gametophytes showed developmental delay, with female gametophytes displaying unfused polar nuclei (8.2%). Additionally, 4.3% of all female gametophytes observed showed an aberrant egg apparatus, with mispositioned synergid nuclei (Fig. 1). A small fraction of female gametophytes were found collapsed but in a proportion similar to the one observed for WT pistils (less than 1%). Similar phenotypes and distribution were observed when *adxr-2*/*ADXR* pistils were analyzed (*SI Appendix*, Fig. S2). In addition, we studied WT pollen tube attraction in *adxr*/*ADXR* pistils by aniline blue staining. When WT pistils were analyzed, 90.7 ± 3.06% of the ovules analyzed showed a pollen tube reaching the micropyle ($n$ = 10 pistils, 231 ovules quantified). The percentage was 83.7 ± 4.72% for ovules in *adxr-1*/*ADXR* pistils ($n$ = 5 pistils, 92 ovules quantified, $P$ = 0.0006, $t$ test) and 86.2 ± 3.77% in *adxr-2*/*ADXR* pistils ($n$ = 5 pistils, 126 ovules quantified, $P$ = 0.0032, $t$ test). As the percentage of ovules targeted by pollen tubes was slightly but significantly different from WT in the mutants, these results indicate that a small fraction of the ovules carrying defective gametophytes were not attracting pollen tubes and therefore could not be fertilized (*SI Appendix*, Fig. S3).

As the fraction of abnormal female gametophytes observed before pollination could not explain the high ratio of aborted seeds detected in mature siliques, the phenotype of ovules in *adxr*/*ADXR* pistils was studied after fertilization. Self-pollinated pistils of 7 to 8 mm, corresponding to 72 h after pollination (72 HAP), were analyzed. While 93.3% of the embryos analyzed in WT pistils were found at a preglobular to globular stage, *adxr*/*ADXR* pistils showed that only 60% of the embryos analyzed were able to reach that stage (59.7% for *adxr-1*/*ADXR* and 61.4% for *adxr-2*/*ADXR*; *SI Appendix*, Table S3). Embryogenesis was found arrested in 20 to 24% of the ovules analyzed, where development stopped at the zygote or one/two-celled proembryo (Fig. 1 *G–R* and *SI Appendix*, Table S3). In addition, 18.2 and 7.7% of the ovules were found collapsed in *adxr-1*/*ADXR* and *adxr-2*/*ADXR*, respectively. Notably, 7% of the embryos found arrested in *adxr-2*/*ADXR* pistils showed abnormal planes of cell division in the embryo proper (Fig. 1 *H* and *N* and *SI Appendix*, Table S3). To study if such arrest in embryogenesis was due to a gametophytic maternal effect, we crossed both *adxr*/*ADXR* allelic mutants as females using WT plants as pollen donors. The resulting progeny was studied by scoring the number of ovules showing defects in embryogenesis 72 HAP. In both cases, the percentage of ovules showing abnormal embryos found was around 35% (*SI Appendix*, Table S3), indicating that the arrest in embryogenesis observed arises from the female gametophyte, as it is not rescued by WT pollen. Conversely, we crossed WT plants as females, using both *adxr*/*ADXR* allelic mutants as pollen donors. In this case, the percentage of ovules showing abnormal embryogenesis found 72 HAP was around 6%, a value comparable to the one found in hand pollination controls (WT x WT crosses; *SI Appendix*, Table S3). This result indicates that the arrest in embryogenesis observed originates from a defect in the female gametophyte. As the ratio obtained was similar to what is expected from WT crosses, the result also suggests that the slight decrease in TE observed from the male side in reciprocal crosses might be due to a defect in pollen development or pollen tube growth. However, we were not able to find obvious developmental defects when pollen grains were analyzed (*SI Appendix*, Fig. S3). This suggests that the decrease in TE observed might arise from defects in the fertilization process.

ADXs are essential for ADXR activity, as they function as mobile shuttles that transfer electrons between ADXR and a redox partner. In *Arabidopsis*, there are two genes encoding for ADX (*AtADX1* and *AtADX2*) that show high homology

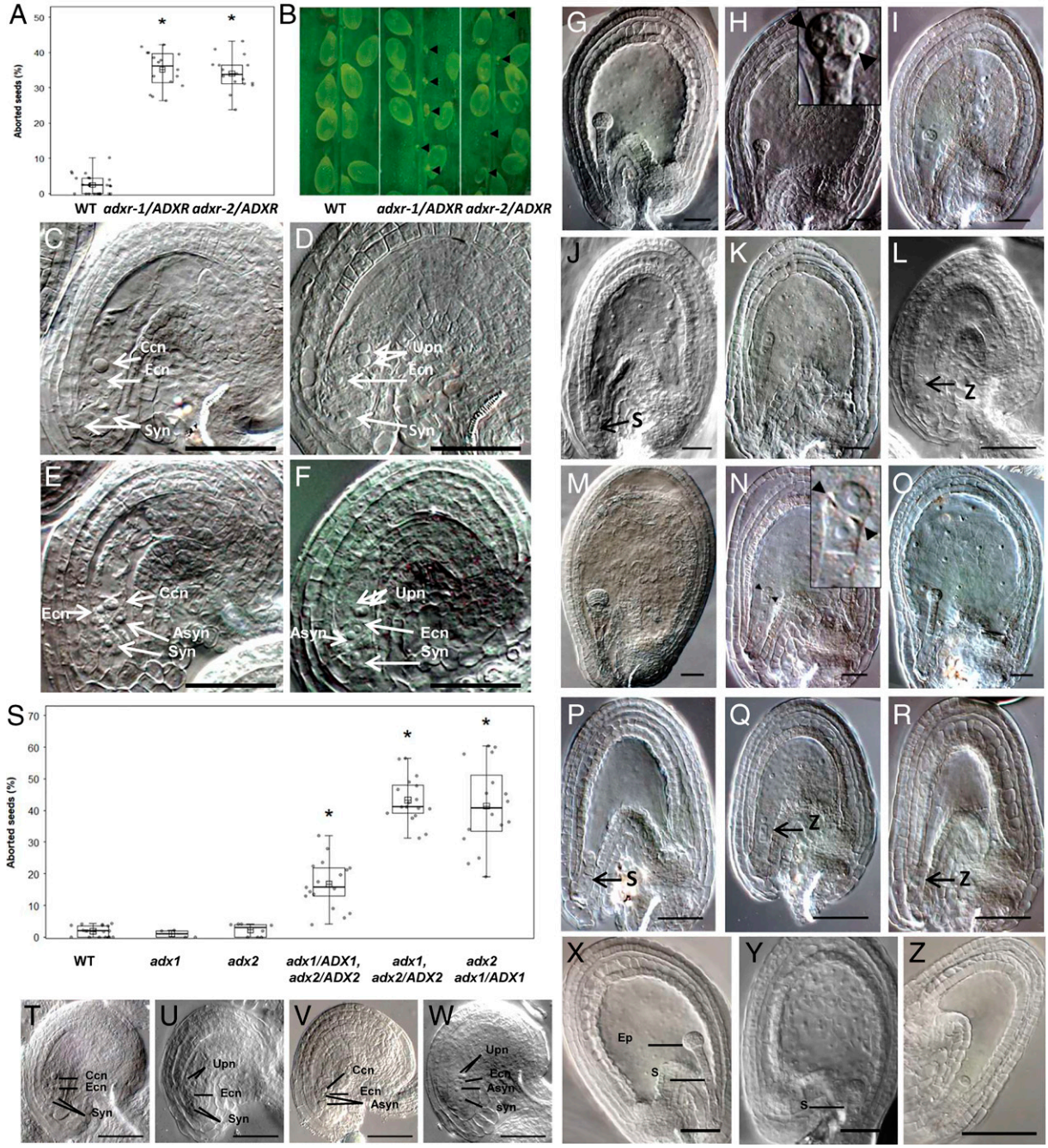


**Fig. 1.** ADXR and ADX1/2 are essential for normal female gametophyte development and embryogenesis in *A. thaliana*. (*A*) Boxplot showing the rate of seeds aborted in WT and mutant plants. Asterisks indicate statistically significant differences from WT, as determined by Welch's two-sample *t* test ($P < 0.01$). (*B*) Stereomicrographs of siliques (arrowheads) at 10 d post fertilization from WT and mutant plants. (*C*) Image of a properly developed female gametophyte found in *adxr-1/ADXR* pistils 48 h after emasculation. (*D*) Female gametophyte showing unfused polar nuclei (upn). (*E*) Female gametophyte showing abnormal polarity in one of the synergid cells (Asyn). (*F*) Female gametophyte showing both an abnormal synergid and unfused polar nuclei. (*G–R*) Ovules were dissected 72 HAP. (*G–L*) Ovules from *adxr-1/ADXR* pistils. (*M–R*) Ovules from *adxr-2/ADXR* pistils. (*G*) Ovule from an *adxr-1/ADXR* pistil showing an embryo at the preglobular stage. (*H*) Embryo at the preglobular stage showing asymmetric divisions in the embryo proper (*Inset*, arrowheads). (*I*) Embryogenesis is arrested at the four-cell stage. (*J*) Embryo showing an aberrant short suspensor (s). Endosperm is developed normally. (*K*) Embryogenesis is arrested at the one-cell stage. (*L*) Fertilized ovule showing embryogenesis arrested at the zygote stage (z). (*M*) Ovule from an *adxr-2/ADXR* pistil showing an embryo at the preglobular stage. (*N*) Embryo at the preglobular stage showing asymmetric divisions in the embryo proper (*Inset*, arrowheads). (*O*) Ovule showing embryogenesis arrested at the four-cell stage. (*P*) Embryo showing an aberrant short suspensor. (*Q*) Fertilized ovule showing embryogenesis arrested at the zygote stage and normal endosperm development. (*R*) Fertilized ovule showing embryogenesis arrested at the zygote stage and no endosperm development. (*S*) Seed abortion rate in WT, *adx1*, *adx2*, and double-mutant plants. Asterisks indicate statistically significant differences from WT, as determined by Welch's two-sample *t* test ($P < 0.01$). (*T–Z*) Ovules from *adx1,adx2/ADX2* pistils were analyzed 48 h after emasculation (*T–W*) or 48 h after pollination (*X–Z*). (*T*) Ovule showing a normal female gametophyte at stage FG7. (*U*) Female gametophyte showing unfused polar nuclei. (*V*) Female gametophyte showing abnormal polarity in one of the synergid cells. (*W*) Female gametophyte showing both an abnormal synergid and unfused polar nuclei. (*X*) Ovule from an *adx1,adx2/ADX2* pistil showing an embryo at the preglobular stage. (*Y*) Embryo showing an aberrant short suspensor. (*Z*) Fertilized ovule showing embryogenesis arrested at the one-cell stage. Ccn, central cell nucleus; Ecn, egg cell nucleus; Ep, embryo proper; syn, synergid cell. (Scale bars, 50 μm.) See also *SI Appendix*, Figs. S1–S4 and Tables S1–S3.

(*SI Appendix*, Fig. S4*A*). To determine whether similar defects to the ones observed in *adxr/ADXR* mutants could be observed in plants impaired in ADX function, single insertional knockout mutants for each gene were examined (*SI Appendix*, Fig. S4 *B–E*). All mutants analyzed show siliques with full seed sets, and no obvious defects in vegetative or reproductive tissues were observed (*SI Appendix*, Fig. S4 *C* and *D*). The absence of phenotypes in *adx1* and *adx2* mutants together with their high sequence similarity suggests that ADX1 and ADX2 might be functionally redundant. To study this possibility, we crossed single *adx* mutants and analyzed the phenotype of plants carrying *adx1,adx2/ADX2* and *adx1/ADX1,adx2* mutant allele combinations, as we were not able to detect double-homozygous plants in the F2 progeny ($n = 254$ plants genotyped). The rate of ovule abortion observed was 16.9% in siliques from *adx1/ADX1 adx2/ADX2* plants, 43.3% in *adx1,adx2/ADX2* siliques, and 39.9% in *adx1/ADX1,adx2* siliques (Fig. 1*S*). As shown by *adxr/ADXR* plants, this phenotype could not be rescued by pollination with WT pollen, suggesting a maternal effect (*SI Appendix*, Table S4). In addition, female gametophytes and embryos showed defects that were similar to the ones observed in *adxr/ADXR* plants (Fig. 1 *T–Z*).

***ADXR* Is Expressed in Gametophytic and Young Sporophytic Tissues.** To study the temporal and spatial expression pattern of *ADXR* during different stages of the plant life cycle, we analyzed transgenic plants carrying an *ADXR* promoter–*GUS* reporter gene fusion (*pADXR-GUS*). The sequence used as the *ADXR* putative promoter was the complete intergenic region located upstream of the *ADXR* ATG codon (640 bp). GUS expression was detected in regions of active cell division in the young seedlings in the hypocotyl, cotyledons, and leaf primordia (Fig. 2 *A–D*). In mature leaves as well as in sepals, expression was weaker and mainly confined to vascular tissues. High expression was also detected in the filaments of mature flowers (Fig. 2*E*). GUS expression was also detected in mature pollen grains (Fig. 2*F*) and mature female gametophytes, associated with the egg apparatus and central cell (Fig. 2*G*). After fertilization, GUS activity was detected in the zygote and until the one-cell embryo stage (Fig. 2 *H* and *I*). GUS activity was not detected at later stages of embryogenesis (Fig. 2*J*). To further know the basis of the maternal effect observed, we crossed WT plants with homozygous pADXR-GUS plants and studied GUS staining after fertilization. As can be observed in *SI Appendix*, Fig. S5, while GUS staining was detected from the maternally inherited allele in the zygote, no signal was detected when GUS staining was assayed to look for expression of the paternally inherited allele. This result suggests that the paternal *ADXR* allele is probably not expressed in the embryo or endosperm, at least before the globular stage.

To analyze ADXR localization in the female gametophyte, the fusion protein ADXR-GFP (green fluorescent protein) was followed in transgenic WT plants carrying the construct *pADXR:ADXR-GFP*. This construct was proven to be fully functional as it was able to complement the phenotype observed in *adxr-1/ADXR* plants (*SI Appendix*, Table S5). In ovules, ADXR-GFP was detected both in the integuments of the ovule, in the nucellus, and inside the female gametophyte, mostly in the egg cell and the central cell, associated with mitochondria (Fig. 2 *K* and *L*).

**ADXR–ADX Shuttle Dysfunction Does Not Affect Reactive Oxygen Species Levels or Mitochondrial Functional Status.** One possible consequence of a failure in electron transport is reactive oxygen species (ROS) accumulation, which might well result in developmental arrest as previously described (8). To explore that possibility, ROS levels were analyzed using the ROS-sensitive probe $H_2$DCFDA and quantifying the fluorescence found inside the female gametophytes of pistils from WT, *adxr/ADXR*, and *adx1,adx2/ADX* plants. No significant differences were found (*SI Appendix*, Fig. S6*A*), indicating that ROS production/accumulation was not altered in the mutant female gametophytes. In addition, we assessed whether ADXR–ADX shuttle dysfunction might affect mitochondrial membrane potential/health by using the membrane potential ($\Delta\psi$m) indicator JC-1. While in functional mitochondria with high $\Delta\psi$m, JC-1 spontaneously forms red fluorescent complexes, it remains as a green monomer in unhealthy mitochondria (8). As can be observed in *SI Appendix*, Fig. S6*B*, gametophytic mitochondria from each of the pistils analyzed showed similar distributions of red to green values, suggesting that mitochondrial $\Delta\psi$m was not affected by the mutations examined.

**ADX1 Interacts with Mitochondrial Cytochrome P450s.** As no ROS accumulation nor mitochondrial dysfunction was found in *ADXR* and *ADX* mutant gametophytes, we decided to identify putative redox partners of the ADXR–ADX shuttle by means of a high-throughput yeast two-hybrid screening using ADX1 as a bait (Hibrigenics Services). Among the putative interacting proteins identified, there were clones with a predicted or a reported localization that was associated either with the plasma membrane or with different organelles such as plastids, chloroplasts, or mitochondria (*SI Appendix*, Table S6). As one of the clones identified corresponded to the P450 cytochrome CYP711A1, we decided to investigate if ADX1 can indeed interact with a cytochrome P450 as occurs in animal systems. Thus, we first analyzed if CYP711A1 can be found in mitochondria by analyzing the localization of a CYP711A1-GFP fusion protein using a transient expression system in *Nicotiana benthamiana* and the mitochondrial selective dye MitoTracker red (Invitrogen). As can be observed in Fig. 3*A*, CYP711A1-GFP colocalizes with MitoTracker red, indicating its mitochondrial localization. In addition, to confirm ADX1–CYP711A1 interaction, we performed a bimolecular fluorescence complementation (BiFC) assay using transient expression in *N. benthamiana*. We fused CYP711A1 and ADX1 to N- and C-terminal yellow fluorescent protein (YFP) fragments to generate *CYP711A1-nYFP* and *ADX1-cYFP* fusion constructs under control of the UBQ10 promoter. After *Agrobacterium* infiltration of *N. benthamiana* leaves, YFP signal was strongly detected, indicating ADX1–CYP711A1 interaction (Fig. 3*B*).

The analysis of two allelic insertional mutant lines with a T-DNA insertion in *CYP711A1* [lines CS9564 and CS717630 (9)], however, showed that homozygous *cyp711a1* plants did not show any gametophytic defect, only a slight increase in lateral branching as already reported (10) (*SI Appendix*, Fig. S8 *A–D*). This suggests that other P450 cytochromes might function redundantly with CYP711A1 in *Arabidopsis* mitochondria, thus replacing the CYP711A1 role in loss-of-function mutants.

The *Arabidopsis* genome encodes for 244 P450 genes and 28 pseudogenes (11). However, apart from CYP711A1 shown here (Fig. 3*A*), there are no reports so far that locate any of the other 243 *Arabidopsis* cytochrome P450s in mitochondria. To identify putative mitochondrial P450 cytochromes, we applied 10 different bioinformatics approaches based on sequence characteristics (presence of an N-terminal mitochondrial targeting sequence and other features that direct proteins to mitochondria). The programs used were TargetP, Mitoprot2, SubLoc, iPSORT, Predotar, MitoPred, PeroxP, MultiLoc, WoLFPSORT, and LOCtree. We were able to identify eight candidates that showed different putative localizations according to the software applied (*SI Appendix*, Table S7). We selected the first four candidates shown in *SI Appendix*, Table S7 to evaluate if they were indeed localized in mitochondria. We designed C-terminal translational fusion constructs for each protein with GFP under the control of the CaMV 35S promoter and subcellular

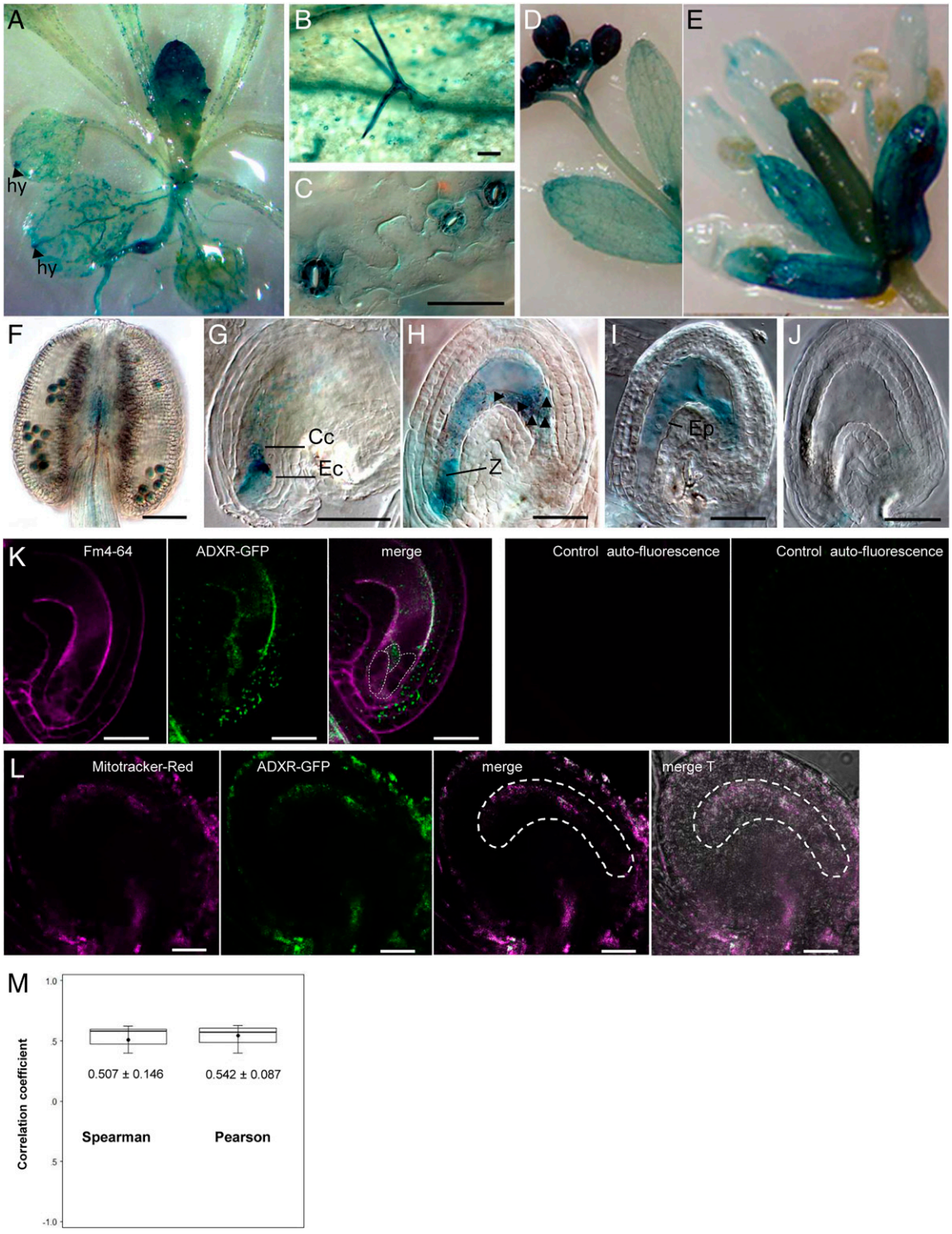


**Fig. 2.** ADXR is expressed in gametophytic and young sporophytic tissues. (*A–J*) Histochemical localization of GUS activity in transgenic *Arabidopsis* plants harboring the pADXR-GUS construct. (*A*) GUS expression observed in a 21-d-old seedling showing expression in hydathodes (hy), vascular tissue, vegetative meristem, and young leaves. (*B*) Expression in a trichome. (*C*) GUS expression is observed in guard cells. (*D*) GUS expression is shown in a young inflorescence. (*E*) Open flower at stage 12 showing GUS staining in sepals, petals, and pistil. (*F*) Anther showing GUS-stained pollen grains. (*G*) Female gametophyte showing GUS expression associated with the egg cell (Ec) and central cell (Cc). (*H*) Fertilized female gametophyte showing GUS staining in the zygote and in the developing endosperm. Arrowheads point to endosperm nuclei. (*I*) GUS staining is still detectable at the one-cell embryo stage, both in the embryo proper (Ep) and in the developing endosperm. (*J*) GUS staining is no longer detectable at the two-cell embryo stage. (*K*) ADXR-GFP is detected inside the female gametophyte, mostly associated with the egg cell and the central cell. FM4-64 staining was used to underline the cells composing the female gametophyte. The pictures shown correspond to the same single confocal slice. Egg apparatus cells are outlined. Controls of autofluorescence display a representative picture of an ovule from a plant that does not carry the GFP fusion construct. Both channels are shown. (*L*) Representative confocal images showing a female gametophyte expressing ADXR-GFP stained with MitoTracker red. The pictures shown correspond to the same single confocal slice. (*M*) Boxplots showing the results of the colocalization analyses of ADXR-GFP and MitoTracker red performed by using the correlation test (PSC) plug-in for ImageJ after background subtraction. As an example, the ROI used is delimited in *L*. Scale bars are 50 μm in *F–J* and 25 μm in *K–L*. See also *SI Appendix*, Figs. S5 and S7.

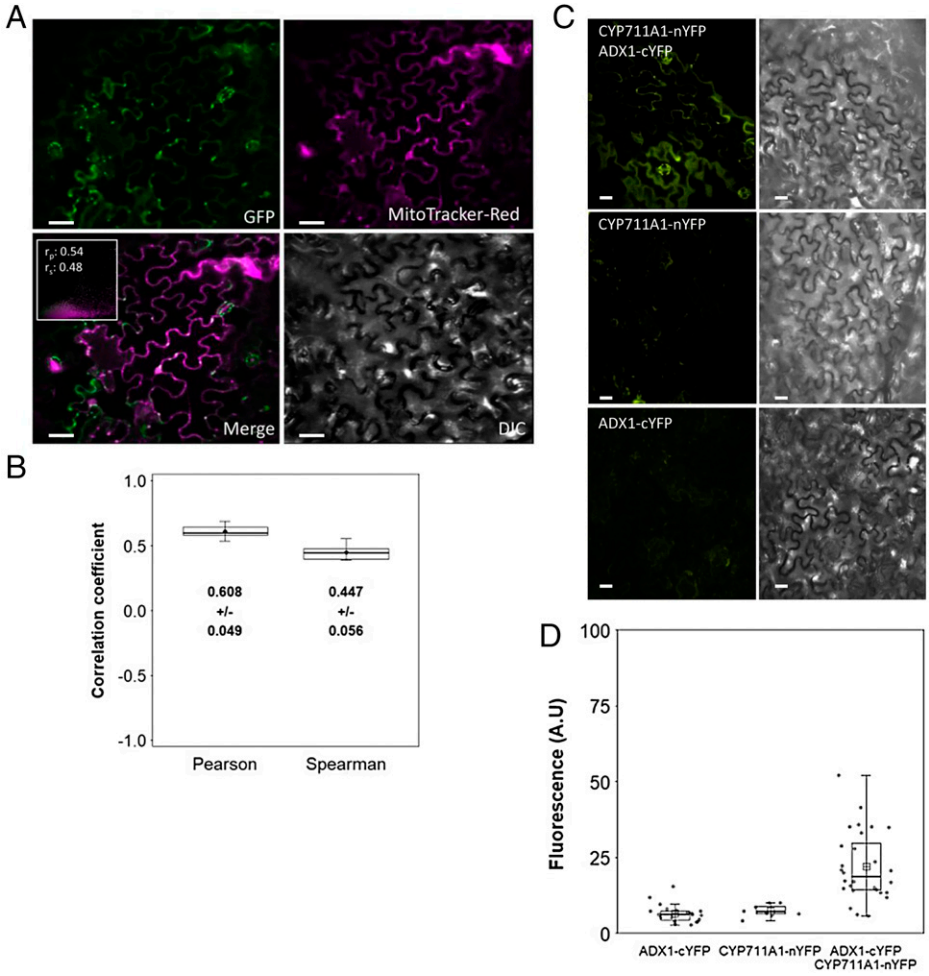


**Fig. 3.** CYP711A1 localizes to mitochondria and interacts with ADX1. (*A*) Representative confocal images showing *N. benthamiana* epidermal cells transiently expressing CYP711A1-GFP and stained with MitoTracker red. (*B*) Boxplots showing the results of the colocalization analyses of CYP711A1-GFP and MitoTracker red performed by using the correlation test (PSC) plug-in for ImageJ after background subtraction. Quantification was performed in at least four ROIs per photo. Three photos were taken per assay. (*C*) BiFC assay: representative microphotographs showing reconstituted YFP fluorescence or DIC images of *N. benthamiana* epidermal cells transformed with plasmids harboring the indicated constructs (CYP711A1-nYFP, ADX1-cYFP, or both). (Scale bars, 50 μm.) (*D*) Boxplots showing YFP fluorescence intensity values obtained in the BiFC assays. Quantification was performed in at least four ROIs per photo. Three photos were taken per assay. The BiFC assays were independently repeated at least three times. A.U., arbitrary units.

localization was studied using a transient expression system in *N. benthamiana* and MitoTracker red. Three of the four candidates analyzed were found to colocalize with MitoTracker red. CYP90A1 (CPD), CYP90D1, and CYP75B1 (TT7) localize in mitochondria while CYP89A2 does not (Fig. 4*A*). To test whether these cytochromes found in mitochondria are able to interact in vivo with ADX1, we performed a BiFC assay, as described for CYP711A1. After *Agrobacterium* infiltration of *N. benthamiana* leaves, a strong YFP signal was detected for CYP90A1 and CYP75B1, while control *N. benthamiana* leaves and leaves infiltrated with constructs to detect ADX1 interaction with CYP90D1 did not show BiFC signal (Fig. 4*B*).

Altogether, these results indicate that ADX1 can interact in vivo with at least three mitochondrial P450s: CYP711A1, CYP90A1, and CYP75B1. To further investigate if these interactions can potentially take place in the female gametophyte, we investigated the expression patterns of *CYP711A1*, *CYP90A1*, and *CYP75B1* by constructing their promoter reporter lines, *CYP711A1::GFP*, *CYP90A1::GFP*, and *CYP75B1::GFP*, respectively. As can be observed in *SI Appendix*, Fig. S7, the three genes are expressed in the sporophytic tissues of the ovule and in the female gametophyte. Additionally, we were able to study ADX1, CYP711A1, and CYP90A1 protein localization inside the female gametophyte using translational fusions with GFP and the mitochondrial probe MitoTracker red (Invitrogen). The three proteins were found inside the female gametophyte and associated with mitochondria (*SI Appendix*, Fig. S7). Thus, both the expression patterns observed and the localization of the proteins studied strongly indicate that the interactions detected can occur inside the female gametophyte.

**Functional Characterization of Mitochondrial P450s Interacting with ADX1.** As we did for *CYP711A1*, single-knockout mutants for each of the genes encoding for *CYP75B1* and hemizygous plants for *CYP90A1* [as homozygous plants are not fertile (12)] were studied to analyze if they showed a defect similar to the ones described for *adx* or *adxr* mutants. However, seed sets were normal for *CYP90A1* mutants and only slightly lower than WT for *CYP75B1* mutants, suggesting functional redundancy (*SI Appendix*, Fig. S8). To study if that was the case, we constructed double mutants crossing each of the mutant lines available, obtaining three combinations of double-hemizygous mutants in F1 (*cyp711a1*/*CYP711A1 cyp90a1*/*CYP90A1*; *cyp711A1*/

*CYP711A1 cyp75b1/CYP75B1*; and *CYP90A1/cyp90a1 cyp75b1/CYP75B1*). When siliques from selfed double-hemizygous plants were analyzed, only slight differences were found between WT plants and single or double mutants (Table 1 and *SI Appendix*, Fig. S8 *A–P*). Triple-mutant plants *cyp711a1 cyp90a1/CYP90A1 cyp75b1* were obtained, as *cyp90a1* homozygous mutants are unfertile and extremely affected. As can be observed in Table 1, triple mutants showed 33.51% ovule abortion, a percentage significantly higher than the one observed in double mutants and close to the maximum of 50% expected if the three mutated alleles present in a female gametophyte were causing a defect with 100% penetrance. To check if the same phenotypes observed in *adxr/ADXR* and *adx* mutant plants were also present in these triple mutants, we analyzed unfertilized and fertilized ovules (*SI Appendix*, Fig. S8 *Q–V*). When ovules were studied 48 h after emasculation, 58.33% of the female gametophytes were found at FG7 stage (mature normal female gametophyte), 25% were observed with unfused polar nuclei, 5.55% presented abnormal egg apparatuses, and 11.11% were found collapsed ($n = 36$). At 72 HAP with WT pollen, embryogenesis showed significant abnormalities. While 62.68% of the ovules presented an embryo at early globular stage, 9.52% of the fertilized ovules were found arrested at the zygote stage, 0.79% were found at a two/four-cell stage with an abnormal short suspensor, and 13.48% presented abnormal planes of cell division (*SI Appendix*, Table S8).

Additionally, we studied WT pollen tube attraction in WT and triple-mutant plants *cyp711a1 cyp90a1/CYP90A1 cyp75b1* by aniline blue staining (*SI Appendix*, Table S9). Although most *cyp* triple-mutant ovules are able to attract pollen tubes, there is a slight but significant difference when compared with WT ovules (88 ± 5.77 vs. 94.7 ± 6.06%, $P = 0.0399$, $t$ test). However, 35.43 ± 9.16% of targeted ovules looked smaller/arrested in comparison with ovules in the same pistil (*SI Appendix*, Table S9), suggesting that even when most ovules are able to attract pollen tubes, seed development is arrested in the triple mutant, as previously shown by differential interference contrast (DIC) microscopy and silique analyses. Altogether, these results suggest that ADXR, ADX, and the P450 cytochromes studied were involved in the same physiological/developmental pathway during female gametophyte development/function and early embryogenesis.

**Steroid Profile of *Arabidopsis* Ovules in WT and *adxr/ADXR* Mutant Plants.** Since ADX1 was found to interact with mitochondrial P450 cytochromes, we decided to address if the ADX–ADXR shuttle was involved in steroid biosynthesis, as described in animal systems. As a first approach, we harvested pistils at stage 14 (13) from

WT and *adxr/ADXR* mutant plants and attempted to detect brassinosteroids (BRs) in pistil extracts using an enzyme-linked immunosorbent assay. However, we were not able to detect steroids in these extracts by this method, suggesting that steroids, if present, might occur at very low concentrations. As steroids present in ovules might be diluted if we used pistil extracts, we decided to directly collect *Arabidopsis* ovules to identify and measure, if possible, the BRs present.

Because *SPOROCYTLESS* (*SPL*) is required for megasporogenesis initiation, *spl* ovules lack a female gametophyte (14). Thus, by comparing WT and *spl* ovules, it would be possible to differentiate steroids present in the sporophytic maternal tissues and the ones that are specific to the female gametophyte. To perform this experiment, we harvested ovules from pistils at stage 14 (13) using custom-designed equipment that suctions and immediately freezes the ovules inside a collecting tube (*Materials and Methods*). Around 40 to 90 mg of ovules was extracted from plants of the indicated genotypes and BRs were analyzed using ultra-high-performance liquid chromatography–tandem mass spectrometry (UHPLC–MS/MS). As the *spl* mutant is in the *Landsberg erecta* (Ler) background, WT plants of the corresponding ecotype were used to compare the steroid content. While BRs like brassinolide, 24-*epi*brassinolide, 24-*epi*-castasterone, and 28-*nor*castasterone were not detected, castasterone and principally homocastasterone were found in ovules from both WT and *spl* plants. Homocastasterone content in *spl* ovules was lower than the levels found in WT ovules (Table 2). This result indicates that homocastasterone contribution in WT ovules was mainly from the female gametophyte. Specifically, the contribution of homocastasterone from the female gametophyte seems to be around 75%, while the sporophytic tissues of the ovule account for the remaining 25% (Table 2). To study if homocastasterone levels in the female gametophyte are dependent on ADXR, we measured the steroid content in ovules from *adxr-1/ADXR* and WT plants (ecotype Col-0, *adxr-1/ADXR* background). In this case, we expect only half of the ovules collected from *adxr-1/ADXR* plants to have ADXR activity in their female gametophytes, while the other half would not, assuming that the mutation is fully penetrant. The contribution of homocastasterone from the sporophytic tissues should be maintained. The value obtained (0.42 ± 0.09 pmol per gram fresh weight [gFW]) is similar to the expected value if ADXR is required for homocastasterone biosynthesis, assuming full penetrance of the mutation in a mix of 50:50 of *adxr* and *ADXR* female gametophytes (0.455 ± 0.085 pmol/gFW; $P = 0.7914$, $t$ test; Table 2). These results suggest that ADXR activity is required for homocastasterone biosynthesis in the female gametophyte.

**Exogenous Homocastasterone Treatment Partially Rescues the Phenotype of ADXR and Cytochrome P450 Mutants.** To investigate whether the gametophytic phenotypes observed were due to low levels of BRs, pistils from WT and *adxr/ADXR* and *cyp711a1,cyp90a1/CYP90A1,cyp75b1* mutant flowers were treated every 24 h with homocastasterone, homobrassinolide, 24-*epi*brassinolide, or a mock solution from stage 9 to stage 14, allowing self-pollination. When mature siliques were scored for abortions, a significant reduction in the rate of ovule abortion was observed in siliques from mutant flowers treated with homocastasterone in comparison with mock-treated plants (Fig. 5). No significant differences were observed when pistils were treated with homobrassinolide or 24-*epi*brassinolide. Although the rescue obtained after homocastasterone treatment was partial, this is likely a reflection of an inefficient uptake of the hormone by the female gametophytes. While BRs were administered to the pistils, they are required inside the female gametophytes, which are enclosed by the maternal tissues of the ovule.

Collectively, our results suggest that homocastasterone might be the bioactive BR required for normal development and function of the female gametophyte in *A. thaliana* and that the ADX–ADXR–P450 shuttle is involved in its biosynthetic pathway inside the gametophytic mitochondria.

## Discussion

Our results show that the ADX–ADXR shuttle is essential for normal development and function of the female gametophyte in *A. thaliana*. The only role attributed so far to ADXs and ADXR is related to biotin biosynthesis. In association with BIO2, ADX and ADXR constituted a reduction system that allowed the formation of an in vitro plant biotin synthase complex (6). However, mutants deficient in biotin are impaired during late embryogenesis [globular to early cotyledon stages (15, 16)] while mutants impaired in ADXR or ADX show phenotypes related to female gametophyte development and function, indicating that these proteins might be also involved in other pathways that are required earlier during development. This is actually not surprising, as ferredoxin reductase–ferredoxin electron transfer systems are considered to be functionally promiscuous

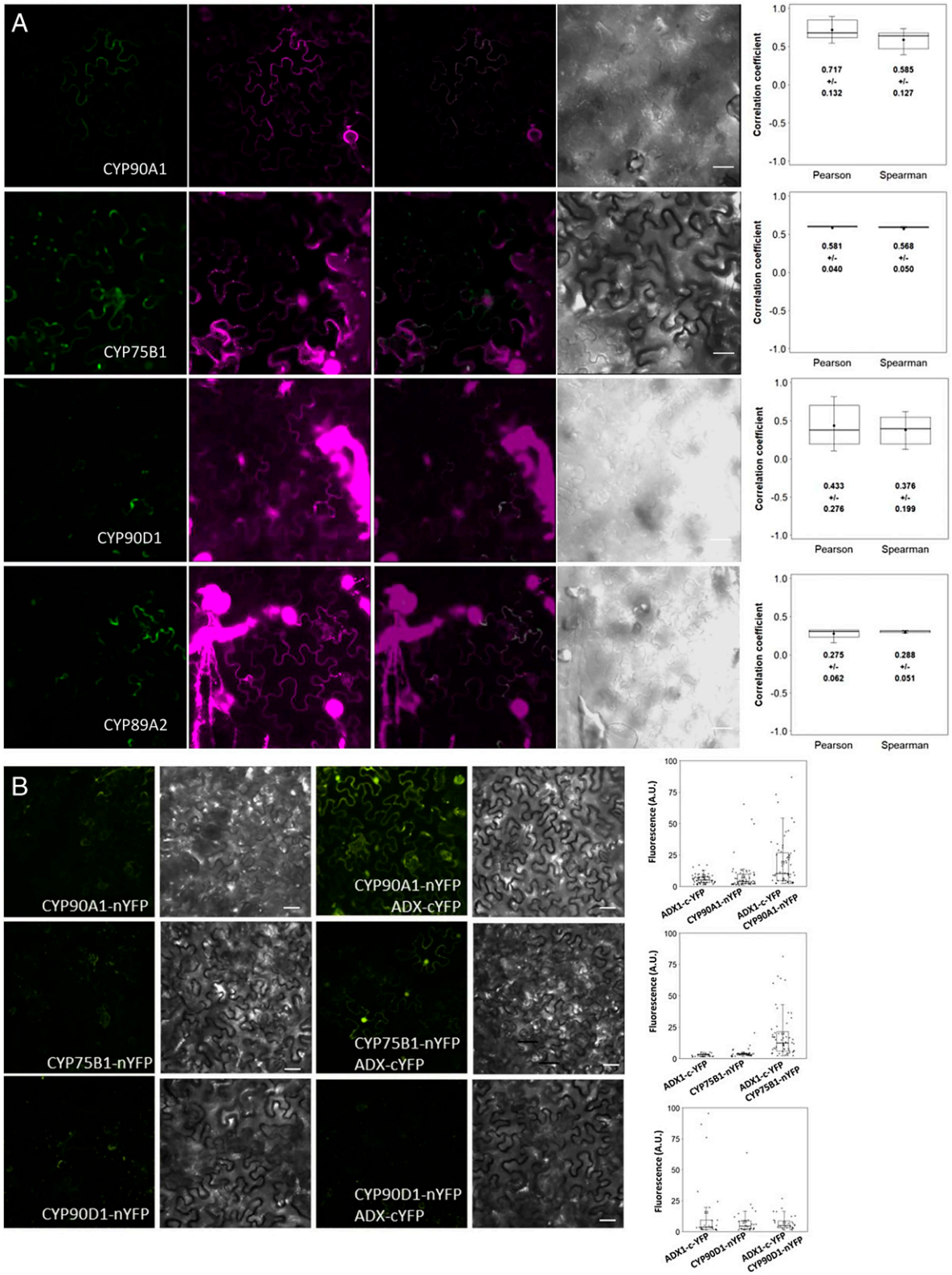


**Fig. 4.** Mitochondrial cytochrome P450s CYP90A1 and CYP75B1 interact with ADX1. (*A*) Representative images showing *N. benthamiana* epidermal cells stained with MitoTracker red transiently expressing the indicated P450-GFP fusions. Boxplots show the results of the colocalization analyses of CYP-GFP fusion proteins and MitoTracker red performed by using the correlation test (PSC) plug-in for ImageJ after background subtraction. Quantification was performed in at least four ROIs per photo. Three photos were taken per assay. (*B*) BiFC analysis of ADX1 interaction with candidate mitochondrial cytochrome P450s. ADX1 and the P450 candidates were fused to the C- and N-terminal YFP fragments to generate ADX1-cYFP and P450-nYFP fusion constructs. The figure shows representative microphotographs displaying reconstituted YFP fluorescence in *N. benthamiana* epidermal cells transformed with plasmids harboring the P450-nYFP constructs alone or together with the ADX1-cYFP construct. Boxplots show YFP fluorescence intensity values obtained in the BiFC assays. Quantification was performed in at least four ROIs per photo. Three photos were taken per assay. The BiFC assays were independently repeated at least three times. (Scale bars, 40 μm.)

**Table 1. Quantification of abortions observed in simple and multiple mutants for genes encoding mitochondrial P450s that interact with ADX1**

| Genotype | *N* (pistils analyzed) | % ovule abortion* |
|---|---|---|
| WT | 25 | 0.99[a] |
| *cyp711a1* | 25 | 1.38[a] |
| *cyp90a1/CYP90A1* | 25 | 1.41[a] |
| *cyp75b1* | 30 | 2.08[ab] |
| *cyp711a1/CYP711A1cyp90a1/CYP90A1* | 25 | 1.12[a] |
| *cyp711a1/CYP711A1cyp75b1/CYP75B1* | 25 | 3.02[b] |
| *cyp90a1/CYP90A1cyp75b1/CYP75B1* | 25 | 3.44[b] |
| *cyp711a1cyp90a1/CYP90A1cyp75b1* | 15 | 33.51[c] |

*Different letters indicate significant differences ($P < 0.05$) shown by the Kruskal–Wallis test with Dunn's post hoc test. Multiple testing was corrected by using the Bonferroni method.

and might serve as an electron shuttle for a variety of substrates (17, 18). Among the phenotypes observed for the mutants studied, the presence of unfused polar nuclei is noticeable. Remarkably, a great number of mutants impaired in mitochondrial proteins show this defect, suggesting that mitochondrial functions are essential for nucleus fusion; that is the case for NFD1 (19), the mitochondrial cysteinyl–transfer RNA synthetase SYCO ARATH (20), a mitochondrial chaperone, ortholog of yeast MDJ1 (21), and an Mn-dependent mitochondrial superoxide dismutase (8, 22). However, the majority of *adxr* and *adx* mutant female gametophytes show a gametophytic maternal effect. While gametophytes can be fertilized, embryogenesis is arrested very early and the phenotype cannot be rescued by pollination with WT pollen. As WT pollen is not able to rescue the embryogenesis arrest observed and *ADXR* is expressed only from the maternal side, our results suggest that an ADXR-dependent signal from the female gametophyte is essential to sustain early embryogenesis.

In animals, ADX–ADXR activity is related to steroidogenesis, transferring electrons from NADPH to a mitochondrial cytochrome (commonly referred to as P450scc) that catalyzes the cleavage of cholesterol to pregnenolone (23, 24). However, as no mitochondrial P450s were described so far in plants, steroidogenic activity has never been related to mitochondria. In this work, we demonstrated the presence of four *Arabidopsis* cytochrome P450s in mitochondria (CYP711A1 or MAX1, CYP90A1 or CPD, CYP90D1, and CYP75B1 or TT7). Three of them were shown to interact with ADX1 in vivo (CYP711A1, CYP90A1, and CYP75B1), suggesting that the mitochondrial ADXR–ADX–P450 shuttle might be functional in *Arabidopsis*. Triple mutants impaired in CYP711A1, CYP90A1, and CYP75B1 showed characteristics of *adxr* and *adx* mutants, with female gametophytes displaying unfused polar nuclei and arrested embryogenesis. Altogether, these results indicate that CYP711A1, CYP90A1, or CYP75B1 might be able to function as redox partners for the ADX–ADXR electron shuttle and that they are involved in the same developmental process.

When steroid content was measured in ovules, homocastasterone was the most abundant steroid found (Table 2). Significantly, *spl* ovules (which lack a female gametophyte) contain considerably lower levels of homocastasterone than WT, indicating that homocastasterone is predominantly located in the female gametophyte (Table 2). As the homocastasterone levels found in ovules from *ADXR/adxr* plants were lower than those found in WT ovules, our results suggest that ADXR activity is required for homocastasterone biosynthesis. To further test this hypothesis, we conducted an experiment to determine if different steroids were able to rescue the phenotype observed in mutants for ADXR and the mitochondrial P450 found to interact with ADX1. While 24-*epi*brassinolide and homobrassinolide were not able to rescue the mutant phenotype, the exogenous application of homocastasterone partially rescued the seed set of the mutant siliques, indicating that ADXR and the studied cytochrome P450s might be involved in homocastasterone biosynthesis and that the phenotype observed was due to a deficiency in this hormone. In addition, this experiment indicates that homocastasterone, specifically, is the BR required for normal megagametogenesis and early embryogenesis.

Taking into account all these results, we postulate a model in which homocastasterone biosynthesis takes place in the female gametophyte mitochondria, in a pathway that involves an ADXR–ADX–P450 electron shuttle as occurs in animal systems, and whose activity is essential for female megagametophyte development and function (Fig. 6). In this model, a sterol, which can be campesterol or sitosterol, as they are common precursors for BR biosynthesis (25), might be imported into the inner mitochondrial membrane via PBR, a peripheral-type benzodiazepine receptor that was shown to regulate sterol transport from the outer to the inner mitochondrial membrane in *Arabidopsis* (23). Inside mitochondria, electrons are transferred from NADPH via ADX–ADXR to one of the P450s that are able to interact with ADX1 and that were found to be required for a functional megagametophyte (CYP711A1, CYP90A1, or CYP75B1). We propose that this electron transfer is essential at least for homocastasterone biosynthesis in the female gametophyte. Although homocastasterone can function as a precursor for castasterone and BR biosynthesis (26), homocastasterone is itself a bioactive molecule. It is able to interact with the BRI1 receptor and thus to be involved in BR-mediated signaling (27). At nanomolar concentrations, BRs are able to promote cell division and elongation and to act synergically with auxins and gibberellins (28–32). In addition, BRs modulate the orientation and stability of microtubules affecting cell-division planes and cell shape (33, 34). These activities can explain the phenotypes observed in the mutants studied. Not only is embryogenesis arrested in these mutants but abnormal planes of cell division were also found in a fraction of the mutant embryos. Homocastasterone in particular has been

**Table 2. Brassinosteroid levels in ovules extracted from the indicated genotypes, pmol/gFW**

| Genotype | Castasterone, mean ± SEM | Homocastasterone, mean ± SEM |
|---|---|---|
| WT Ler | *<LOD* | 1.22 ± 0.12 |
| *Spl* | *<LOD* | 0.32 ± 0.06* |
| WT Col | 0.96 ± 0.13 | 0.74 ± 0.19 |
| *adxr/ADXR* | 0.73 ± 0.12 | 0.42 ± 0.09[†] |

Numbers represent the mean of three replicates. For each experiment, 40 to 90 mg of ovules was harvested from plants of the indicated genotypes and BRs were analyzed using UHPLC–MS/MS. *<LOD* indicates concentrations below the calculated limit of detection.

*Significantly different from WT Ler values (*t* test, $P = 0.0204$).

[†]Similar to the expected value (0.455 ± 0.085) if homocastasterone content in female gametophytes is dependent on ADXR activity, assuming full penetrance of the mutation in a mix of 50:50 of *adxr* and *ADXR* female gametophytes (*t* test, $P = 0.7914$).

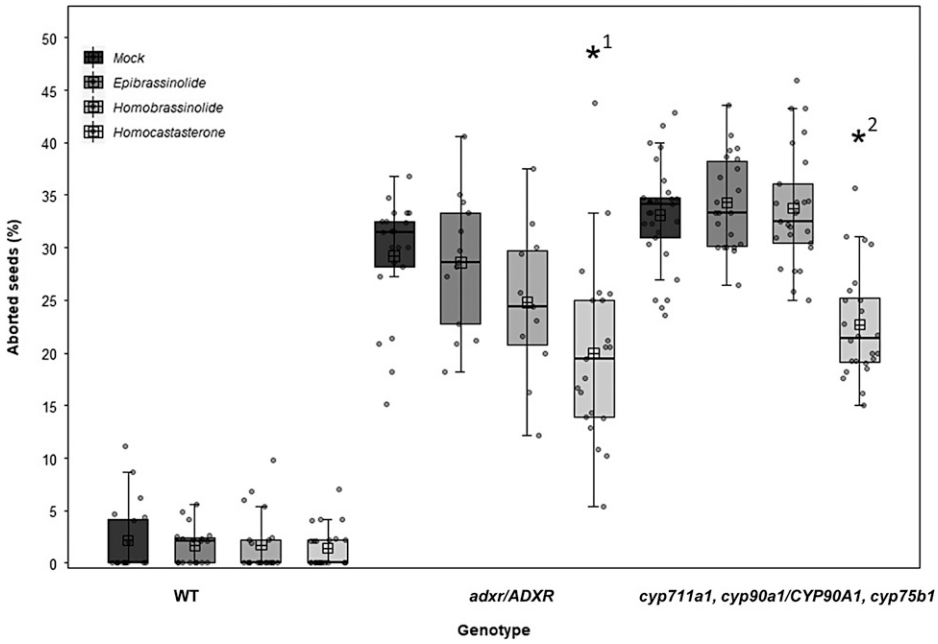


**Fig. 5.** Homocastasterone treatment partially rescues *adxr* and P450 mutant phenotypes. Each box shows the first quartile (lower limit), median (center line), and third quartile (upper limit) and whiskers (extending 1.5 times the interquartile range), while dots show individual data points, including outliers. Small squares inside individual boxes indicate the mean of each group. Asterisks represent statistical differences ($P < 0.001$) in comparison with the mock treatment. $*^1P = 0.000212$, $*^2P = 1.12e\text{-}09$. Calculated $P$ values were determined by Student's $t$ test. Each individual data point corresponds to an analyzed pistil (each containing 40 to 50 ovules).

reported to promote cell expansion in *Arabidopsis* cell cultures (35), which is a crucial process during female gametogenesis and is rapidly induced after fertilization. Taking into account BR biological activities, we propose that homocastasterone biosynthesis through the ADXR–ADX–P450 mitochondrial shuttle might be required in the female gametophyte to sustain early embryo development, mediating both cell division and expansion and cell-division orientation. Altogether, our findings reveal not only a remarkable similarity between steroid biosynthetic pathways in plants and animals but also a common function during sexual reproduction. Although sexual reproduction appeared in eukaryotes before the divergence of plant and animal lineages, it is too early to dissect if these common molecular pathways represent ancestral conserved sexual features or if they are a consequence of convergent evolution.

## Materials and Methods

**Plant Material and Growth Conditions.** All seeds used in this work were obtained from the *Arabidopsis* Biological Resource Center, Ohio State University (9) except for those donated as specified. Plant material and growth conditions are described in detail in *SI Appendix, Materials and Methods*.

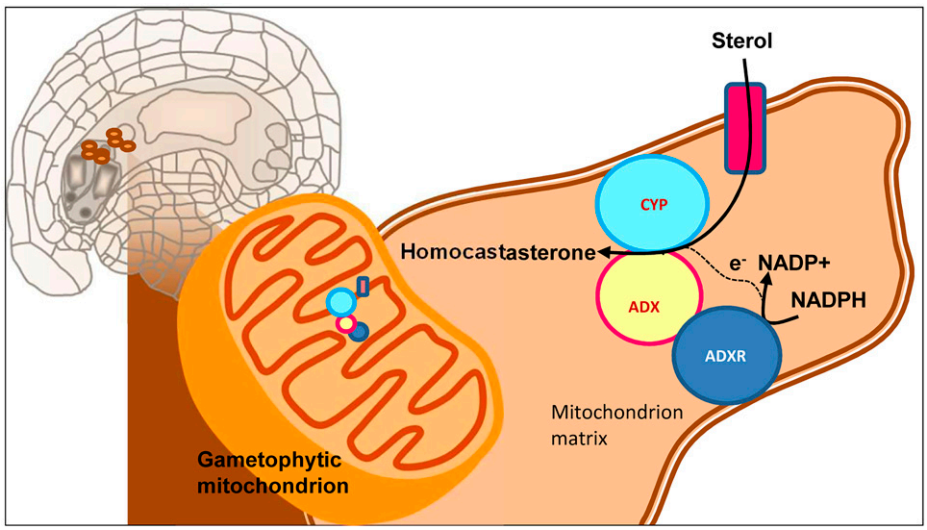


**Fig. 6.** Proposed model showing homocastasterone biosynthesis in mitochondria of female gametophyte cells. Through a sterol transporter, sterols are imported to mitochondria, where electrons transferred from NADPH via the ADXR–ADX electron shuttle are used by a mitochondrial cytochrome (CYP711A1, CYP90A1, or CYP75B1) to synthesize homocastasterone. The synthesis of homocastasterone through this mitochondrial pathway is essential for normal female gametophyte development/function and early embryogenesis in *A. thaliana*.

**Morphological and Histological Analyses.** Pistils from different floral developmental stages were dissected and cleared overnight in Hoyer's solution. For GUS staining, developing carpels and siliques were dissected and incubated in GUS staining buffer as already described (36). Ovules were observed on a Zeiss Axio Imager A2 microscope using DIC optics. Images were captured on an Axiocam HRC charge-coupled device camera (Zeiss) using the Axiovision program (version 4.2). Mitochondrial distribution was studied by using MitoTracker red (Invitrogen) and confocal microscopy. Stock solutions were prepared fresh for each use at 1 mM in dimethyl sulfoxide (DMSO). The working solution was prepared by diluting the stock in phosphate-buffered saline (pH 7.2) to a final concentration of 10 μM. To detect mitochondria in the female gametophytes, the pistils were dissected and incubated in the working solution for 30 min on a microscopy slide at room temperature protected from light. After incubation, pistils were observed using confocal microscopy (Eclipse C1 Plus confocal microscope; Nikon). Images were obtained with EZ-C1 3.80 imaging software and Ti Control. For FM 4-64 (Invitrogen) staining, pistils were dissected and incubated in a 50 μM FM4-64 solution for 45 min on a microscopy slide. After incubation, pistils were immediately observed using confocal microscopy (Nikon Eclipse C1 Plus confocal microscope) using EZ-C1 3.80 imaging software and Ti Control. Laser power was set at 10.5% in all studies. The objective used was Super Fluor 40.0×/1.30/0.22 oil at a working distance of 0.22 μm with Immersol 518F oil (Carl Zeiss). The excitation for GFP was 488 nm; the excitation for FM4-64 red fluorescent protein was 561 nm. The pinhole was set at 33.3 μm.

**Aniline Blue Staining.** Details of aniline blue staining can be found in *SI Appendix, Materials and Methods*.

**Yeast Two-Hybrid Screen and Analysis.** Yeast two-hybrid screening was performed by Hybrigenics Services (http://www.hybrigenics-services.com). Details of the yeast two-hybrid screen can be found in *SI Appendix, Materials and Methods*.

**Colocalization Experiments in *N. benthamiana*.** The complementary DNA (cDNA) of each P450 cytochrome was PCR-amplified using the primers listed in *SI Appendix*, Table S10. Each cDNA was cloned into pENTR TOPO (Gateway technology; Invitrogen) and then recombined into the destination plasmid pMDC83 (37), resulting in a p35S-P450-GFP fusion. *Agrobacterium tumefaciens* strain GV3101 carrying p35S-P450-GFP was infiltrated together with *A. tumefaciens* carrying the p19 helper plasmid (which contains a gene-silencing suppressor) into leaf epidermal cells of 5-wk-old *N. benthamiana* plants; 48 to 72 h after infiltration, sections of infiltrated leaves were incubated with 200 nM MitoTracker red (Invitrogen) for 30 min. Finally, subcellular localization studies were performed on a confocal microscope (Nikon Eclipse C1 Plus). Laser power was set at 5 to 10%. The objective used was Super Fluor 40.0×/1.30/0.22 oil at a working distance of 0.22 μm with Immersol 518F oil (Carl Zeiss). The excitation was 488 nm for GFP and 561 nm for MitoTracker red. The pinhole was set at 33.3 μm. Linear (Pearson's) and nonlinear (Spearman's) correlation coefficients for colocalization analysis were obtained by analyzing the images with the PSC colocalization plug-in (ImageJ). The threshold level was set at 10. At least 10 ROIs were analyzed in each case as indicated.

**Colocalization Experiments in *A. thaliana* Stable Lines.** The $ADXR_{prom}$–$ADXR_{cDNA}$ construct was generated by gene synthesis (GenScript) and cloned into pENTR/TOPO (Invitrogen) using Gateway technology. The resultant plasmid was then subjected to the LR clonase reaction (Invitrogen) using the destination vector pMDC107 (37), which resulted in a translational fusion with GFP. The $CYP_{prom}$–$CYP_{cDNA}$ constructs (for *CYP711A1* and *CYP90A1*) were generated by gene synthesis (GenScript) and cloned into pENTR/TOPO (Invitrogen) using Gateway technology. The resultant plasmids were then subjected to the LR reaction using the destination vector pMDC107 (37), which resulted in a translational fusion with GFP. For the *Pro35S-ADX1$_{cDNA}$-GFP* construct, the ADX1 open reading frame was amplified by proofreading PCR and the amplicon obtained was cloned into pENTR/TOPO (Invitrogen). Its sequence was verified and the resultant plasmid was subjected to the LR reaction using the destination vector pMDC83 (37).

Pistils from homozygous transformed plants were dissected and incubated for 30 min in a solution containing 10 μM MitoTracker red (Invitrogen) as described above (*Morphological and Histological Analyses*) and observed using confocal microscopy (Nikon Eclipse C1 Plus confocal microscope). Stock solutions were prepared fresh for each use at 1 mM in DMSO. After incubation, pistils were observed using confocal microscopy (Nikon Eclipse C1 Plus confocal microscope). Images were obtained with EZ-C1 3.80 imaging software and Ti Control. Laser power was set at 10.5%. The objective used was Super Fluor 40.0×/1.30/0.22 oil at a working distance of 0.22 μm with Immersol 518F oil (Carl Zeiss). The excitation for GFP was 488 nm; the excitation for MitoTracker red was 561 nm. The pinhole was set at 33.3 μm. Linear (Pearson's) and nonlinear (Spearman's) correlation coefficients for colocalization analysis were obtained by analyzing the images with the PSC colocalization plug-in (ImageJ). The threshold level was set at 10. At least 10 Regions of Interest (ROIs) outlining the embryo sac of each embryo sac were analyzed in each case as indicated.

**BiFC Analysis.** In vivo analysis of protein interaction was performed by a BiFC assay. The complete cDNAs corresponding to ADX1 and the P450 cytochromes (see primers in *SI Appendix*, Table S10) were cloned into pENTR TOPO and then recombined into BiFC destination plasmids pUBN-cYFP and pUBC-nYFP, respectively (38). The binary plasmids were then introduced into *A. tumefaciens* strain GV3101. Split nYFP- and cYFP-tagged protein pairs were coexpressed in *N. benthamiana* leaves by *A. tumefaciens*–mediated infiltration. Leaves were examined 48 to 72 h post infiltration using confocal microscopy (Nikon Eclipse C1 Plus) and EZ-C1 3.80 and ImageJ imaging software. Laser power was set at 5 to 15%. The objective used was Super Fluor 40.0×/1.30/0.22 oil at a working distance of 0.22 μm with Immersol 518F oil (Carl Zeiss). The excitation to detect YFP was 515 nm. The pinhole was set at 33.3 μm. Fluorescence intensities were measured using ImageJ imaging software. Quantification was performed in at least four circular ROIs per photo (50 μm in diameter) of *N. benthamiana* epidermal cells transformed with plasmids harboring both constructs (CYP711A1-nYFP and ADX1-cYFP) or in cells transformed with plasmids carrying only one of the constructs (CYP711A1-nYFP or ADX1-cYFP) as negative controls (shown in Figs. 3 and 4). Three photos were taken per assay. The BiFC assay was independently repeated at least three times.

**Extraction and Quantification of Endogenous BRs.** Extraction and quantification of endogenous BRs are described in *SI Appendix, Materials and Methods*.

**Mitochondrial Membrane Potential Studies.** These studies are described in detail in *SI Appendix, Materials and Methods*. In addition, we published a tutorial of this procedure in *Bio-protocol* (39).

**Synthesis of Steroids.** Synthesis of steroids is described in detail in *SI Appendix, Materials and Methods*.

**Rescue Experiments.** Petals and sepals of flowers from stages 9 to 14 (13) were gently opened and pistils were immersed in a working solution containing either 24-*epi*brassinolide (Sigma), homobrassinolide, or homocastasterone at 1 μM or a mock solution containing 1:1,000 DMSO for 5 s every 24 h until stage 14. Mature siliques were then analyzed to score the number of ovule abortions present in each one.

**Quantification and Statistical Analysis.** For each assay, presented values are the mean ± SD of the mean. For each experiment, *n* represents the number of pistils analyzed from at least three different plants. Statistical tests performed are detailed in each experiment (40). Numbers of repetitions and replicates are mentioned for each experiment.

**Data Availability.** All study data are included in the article and/or *SI Appendix*.

**ACKNOWLEDGMENTS.** We thank Dr. Rita Gross-Hardt's lab for the marker lines pAP::NLS_GUS, pCKx7::NLS_GUS, pMEA::NLS_GUS, and pEC1::NLS_GUS; Dr. Ueli Grossniklaus for the marker lines ET1119 and ET884; Dr. Venkatesan Sundaresan for the antipodal marker pAt1g36340:GUS and *spl* line; Dr. Gary Drews for the central cell marker DD65; and Dr. Miklos Szekeres for the *cpd* line. We thank Dr. Mario Arteaga Vazquez, who was very generous sharing his father design for the "Kobulenz," the ovule aspirator. We also thank Daniela Villamonte for technical assistance with confocal microscopy and lab members for helpful discussions. This research was funded by grants to G.C.P. from Agencia Nacional de Promoción Científica y Técnica Argentina (PICT-2016-0110, PICT-2017-0201) and the Howard Hughes Medical Institute (International Early Career Scientist Award 55007430), a grant to A.M.D. from Agencia Nacional de Promoción Científica y Técnica Argentina (PICT-2016-0382), and a grant to D.F.F. from Agencia Nacional de Promoción Científica y Técnica Argentina (PICT-2017-0232). A.M.B. is a postdoctoral fellow of Consejo Nacional de Investigaciones Científicas y Técnicas (CONICET); N.S. and M.M.C. are doctoral fellows of CONICET; and D.F.F., E.J.Z., A.M.D., and G.C.P. are CONICET researchers. The work was also supported by the Ministry of Education, Youth and Sports of the Czech Republic (European Regional Development Fund Project "Plants as a Tool for Sustainable Global Development," CZ.02.1.01/0.0/0.0/16_019/0000827).

1. L. E. Vickery, Molecular recognition and electron transfer in mitochondrial steroid hydroxylase systems. *Steroids* **62**, 124–127 (1997).
2. K. M. Ewen, M. Kleser, R. Bernhardt, Adrenodoxin: The archetype of vertebrate-type [2Fe-2S] cluster ferredoxins. *Biochim. Biophys. Acta* **1814**, 111–125 (2011).
3. W. L. Miller, Minireview: Regulation of steroidogenesis by electron transfer. *Endocrinology* **146**, 2544–2550 (2005).
4. M. R. Freeman, A. Dobritsa, P. Gaines, W. A. Segraves, J. R. Carlson, The dare gene: Steroid hormone production, olfactory behavior, and neural degeneration in *Drosophila*. *Development* **126**, 4591–4602 (1999).
5. K. Takubo *et al.*, Identification and molecular characterization of mitochondrial ferredoxins and ferredoxin reductase from *Arabidopsis*. *Plant Mol. Biol.* **52**, 817–830 (2003).
6. A. Picciocchi, R. Douce, C. Alban, The plant biotin synthase reaction: Identification and characterization of essential mitochondrial accessory protein components. *J. Biol. Chem.* **278**, 24966–24975 (2003).
7. G. C. Pagnussat *et al.*, Genetic and molecular identification of genes required for female gametophyte development and function in *Arabidopsis*. *Development* **132**, 603–614 (2005).
8. M. V. Martin, D. F. Fiol, V. Sundaresan, E. J. Zabaleta, G. C. Pagnussat, oiwa, a female gametophytic mutant impaired in a mitochondrial manganese-superoxide dismutase, reveals crucial roles for reactive oxygen species during embryo sac development and fertilization in *Arabidopsis*. *Plant Cell* **25**, 1573–1591 (2013).
9. J. M. Alonso *et al.*, Genome-wide insertional mutagenesis of *Arabidopsis thaliana*. *Science* **301**, 653–657 (2003).
10. G. Lazar, H. M. Goodman, MAX1, a regulator of the flavonoid pathway, controls vegetative axillary bud outgrowth in *Arabidopsis*. *Proc. Natl. Acad. Sci. U.S.A.* **103**, 472–476 (2006).
11. S. Bak *et al.*, Cytochromes P450. *Arabidopsis Book* **9**, e0144 (2011).
12. J. Mathur *et al.*, Transcription of the *Arabidopsis* CPD gene, encoding a steroidogenic cytochrome P450, is negatively controlled by brassinosteroids. *Plant J.* **14**, 593–602 (1998).
13. J. L. Bowman, G. N. Drews, E. M. Meyerowitz, Expression of the *Arabidopsis* floral homeotic gene AGAMOUS is restricted to specific cell types late in flower development. *Plant Cell* **3**, 749–758 (1991).
14. W. C. Yang, D. Ye, J. Xu, V. Sundaresan, The SPOROCYTELESS gene of *Arabidopsis* is required for initiation of sporogenesis and encodes a novel nuclear protein. *Genes Dev.* **13**, 2108–2117 (1999).
15. T. Schneider, R. Dinkins, K. Robinson, J. Shellhammer, D. W. Meinke, An embryo-lethal mutant of *Arabidopsis thaliana* is a biotin auxotroph. *Dev. Biol.* **131**, 161–167 (1989).
16. R. Muralla *et al.*, A bifunctional locus (BIO3-BIO1) required for biotin biosynthesis in *Arabidopsis*. *Plant Physiol.* **146**, 60–73 (2008).
17. P. J. Bakkes *et al.*, Design and improvement of artificial redox modules by molecular fusion of flavodoxin and flavodoxin reductase from *Escherichia coli*. *Sci. Rep.* **5**, 12158 (2015).
18. D. L. Catalano-Dupuy, M. A. Musumeci, A. López-Rivero, E. A. Ceccarelli, A highly stable plastidic-type ferredoxin-NADP(H) reductase in the pathogenic bacterium *Leptospira interrogans*. *PLoS One* **6**, e26736 (2011).
19. M. F. Portereiko *et al.*, NUCLEAR FUSION DEFECTIVE1 encodes the *Arabidopsis* RPL21M protein and is required for karyogamy during female gametophyte development and fertilization. *Plant Physiol.* **141**, 957–965 (2006).
20. C. Kägi, N. Baumann, N. Nielsen, Y.-D. Stierhof, R. Gross-Hardt, The gametic central cell of *Arabidopsis* determines the lifespan of adjacent accessory cells. *Proc. Natl. Acad. Sci. U.S.A.* **107**, 22350–22355 (2010).
21. C. A. Christensen *et al.*, Mitochondrial GFA2 is required for synergid cell death in *Arabidopsis*. *Plant Cell* **14**, 2215–2232 (2002).
22. Y. Bi *et al.*, Production of reactive oxygen species, impairment of photosynthetic function and dynamic changes in mitochondria are early events in cadmium-induced cell death in *Arabidopsis thaliana*. *Biol. Cell* **101**, 629–643 (2009).
23. P. Lindemann *et al.*, A novel *Arabidopsis thaliana* protein is a functional peripheral-type benzodiazepine receptor. *Plant Cell Physiol.* **45**, 723–733 (2004).
24. L. Stryer, *Biochemistry* (W. H. Freeman, New York, 1988), 565–570.
25. S. D. Clouse, Brassinosteroids. *Arabidopsis Book* **9**, e0151 (2011).
26. S. H. Joo, M. S. Jang, M. K. Kim, J. E. Lee, S. K. Kim, Biosynthetic relationship between $C_{28}$-brassinosteroids and $C_{29}$-brassinosteroids in rice (*Oryza sativa*) seedlings. *Phytochemistry* **111**, 84–90 (2015).
27. T.-W. Kim *et al.*, *Arabidopsis* CYP85A2, a cytochrome P450, mediates the Baeyer-Villiger oxidation of castasterone to brassinolide in brassinosteroid biosynthesis. *Plant Cell* **17**, 2397–2412 (2005).
28. J. L. Nemhauser, T. C. Mockler, J. Chory, Interdependency of brassinosteroid and auxin signaling in *Arabidopsis*. *PLoS Biol.* **2**, E258 (2004).
29. K. Tanaka *et al.*, Physiological roles of brassinosteroids in early growth of *Arabidopsis*: Brassinosteroids have a synergistic relationship with gibberellin as well as auxin in light-grown hypocotyl elongation. *J. Plant Growth Regul.* **22**, 259–271 (2003).
30. F. Lozano-Elena, A. Planas-Riverola, J. Vilarrasa-Blasi, R. Schwab, A. I. Caño-Delgado, Paracrine brassinosteroid signaling at the stem cell niche controls cellular regeneration. *J. Cell Sci.* **131**, jcs204065 (2018).
31. W. B. Jiang, W. H. Lin, Brassinosteroid functions in *Arabidopsis* seed development. *Plant Signal. Behav.* **8**, e25928 (2013).
32. M. K. Zhiponova *et al.*, Brassinosteroid production and signaling differentially control cell division and expansion in the leaf. *New Phytol.* **197**, 490–502 (2013).
33. M. Catterou *et al.*, Brassinosteroids, microtubules and cell elongation in *Arabidopsis thaliana*. II. Effects of brassinosteroids on microtubules and cell elongation in the bul1 mutant. *Planta* **212**, 673–683 (2001).
34. X. Liu *et al.*, Brassinosteroids regulate pavement cell growth by mediating BIN2-induced microtubule stabilization. *J. Exp. Bot.* **69**, 1037–1049 (2018).
35. Z. Zhang *et al.*, Brassinosteroids regulate plasma membrane anion channels in addition to proton pumps during expansion of *Arabidopsis thaliana* cells. *Plant Cell Physiol.* **46**, 1494–1504 (2005).
36. G. C. Pagnussat, H. J. Yu, V. Sundaresan, Cell-fate switch of synergid to egg cell in *Arabidopsis eostre* mutant embryo sacs arises from misexpression of the BEL1-like homeodomain gene BLH1. *Plant Cell* **19**, 3578–3592 (2007).
37. M. D. Curtis, U. Grossniklaus, A Gateway cloning vector set for high-throughput functional analysis of genes in planta. *Plant Physiol.* **133**, 462–469 (2003).
38. C. Grefen *et al.*, A novel motif essential for SNARE interaction with the K(+) channel KC1 and channel gating in *Arabidopsis*. *Plant Cell* **22**, 3076–3092 (2010).
39. M. V. Martin, D. F. Fiol, E. J. Zabaleta, G. C. Pagnussat, *Arabidopsis thaliana* embryo sac mitochondrial membrane potential stain. *Bio Protoc.* **4**, e1128 (2014).
40. R Core Team, R: A Language and Environment for Statistical Computing (R Foundation for Statistical Computing, Vienna, Austria, 2019). https://www.R-project.org/.